Supporting Information

Bilbao et al. 10.1073/pnas.1706754115

Analysis of a Roll Resulting from Out-of-Plane Displacements of the Nematode Head

This section provides numerical evidence that an out-of-plane displacement of the nematode head segment alone is insufficient for producing the rapid roll reorientation of the nematode body (observed in our experiments). In our simplified numerical model, a segment of length l_h is displaced out of the undulation plane by a tilt angle

$$\theta^{\text{tilt}}(t) = \theta^{\max} A^{-1} \kappa(s_h + \Delta\phi), \qquad \textbf{[S1]}$$

where $\theta^{\max}$ is the maximal tilt angle, $s_h = v_s t + L$ is the head position at time t, κ is the harmonic curvature function (Eq. **3** in the main text), A is the curvature-wave amplitude, and $\Delta\phi$ is the phase shift between time variation of the head curvature $\kappa(s_h)$ and head tilt.

The tilt is achieved by rotating the head segment about the unit normal vector $\hat{\boldsymbol{n}}$ located at the body coordinate $s' = L - l_h$, that is, at the bead separating the head segment from the rest of the body. As in the main text, $s' = 0$ denotes the coordinate of the tail and $s' = L$ is the coordinate of the head.

Fig. S1 shows the roll rotation rate per undulation period ω^{roll} versus head-length fraction $f_h = l_h/L$ of *C*-shaped nematodes undergoing modulated head tilts, Eq. **S1**, for $\Delta\phi$ and various maximum tilt angles $\theta^{\max}$. The roll rotation rate is well below what is observed in our experiments, even for large $\theta^{\max}$ and $f_h = 0.3$. This value of f_h corresponds to the fraction of the body innervated by the nerve-ring motor neurons (1–3), which is thought of as being capable of 3D movements. Simulations with different values of the phase shift $\Delta\phi$ show that the roll rotation rate associated with the tilt of the head segment does not exceed $60°$.

Application to Chemotaxis

Here we demonstrate that a nematode can efficiently chemotax in 3D using planar turns and roll maneuvers. We focus on the klinokinesis, a chemotaxis strategy in which the nematode varies the frequency of directional changes of its trajectory to achieve longer runs in the favorable direction. The changes of the frequency of turns occur in response to a chemotactic signal associated with the chemoattractant concentration variation. *C. elegans* has been shown to use this strategy in planar chemotaxis when it crawls on an agar surface (4, 5). Our calculations demonstrate that klinokinesis is also effective in 3D undulatory locomotion in which 3D reorientation is achieved via a combination of planar turns and rolls.

In our model, the turn frequency is controlled by the chemotaxis-response signal

$$Q(t) = \int_0^t C(t - t') M(t') dt', \qquad \textbf{[S2]}$$

where $C(t)$ is the chemoattractant concentration at the position of the sensory openings (nematode head). The memory function $M(t')$ in Eq. **S2** decays with time and satisfies the ideal adaptation condition

$$\int_0^\infty M(t') dt' = 0, \qquad \textbf{[S3]}$$

which ensures that there is no response to a constant chemoattractant concentration. In our numerical calculations we use

$$M(t) = \epsilon^2 \mathrm{e}^{-\epsilon t} \left[(\epsilon t) - \frac{1}{2} (\epsilon t)^2 \right], \qquad \textbf{[S4]}$$

where ϵ is the memory–time constant. Eqs. **S2**–**S4** mimic the combined transient response of ON and OFF chemosensory neurons of *C. elegans* to variation in chemoattractant concentration. A similar memory function has been used to describe bacterial run-and-tumble chemotaxis (6).

To represent the experimentally observed sigmoidal response of the turn frequency to the chemoattractant concentration variation (4, 5), we assume that the turn initiation rate $r_s(Q)$ has a region linear in Q and lower and higher turn-rate saturation limits r_s^L and r_s^H,

$$r_s(Q) = \begin{cases} r_s^L; & f(Q) \le r_s^L \\ f(Q); & r_s^L < f(Q) < r_s^H \\ r_s^H; & r_s^H \le f(Q) \end{cases}, \qquad \textbf{[S5]}$$

where

$$f(Q) = r_s^0 \left[1 - \alpha_s Q(t) \right]. \qquad \textbf{[S6]}$$

The parameter r_s^0 is the turn initialization rate in the absence of chemoattractant, and α_s is a chemical sensitivity parameter. The nematode also performs roll maneuvers initiated at a constant rate r_τ^0.

The nematode burrows or swims using the default harmonic-curvature locomotion mode with $A/q \approx 1$ and switches randomly to a turn or roll mode at the corresponding initiation rates $r_s(t)$ and r_τ^0. The gait parameters and chemosensory-control parameters used in our simulations are listed in Table S1. To assess the effect of the nematode gait and dynamics on the chemotaxis efficiency, we use the same chemosensation and turn-rate parameters for the burrowing and swimming cases.

The effectiveness of chemotaxis in 3D is evaluated using a geometry analogous to a typical experimental setup for investigating 2D chemotaxis on an agar surface (7, 8). Accordingly, as depicted in Fig. S2*A*, the nematodes are placed at a designated starting point at the edge of a Gaussian chemoattractant concentration distribution; the chemotaxis efficiency is determined by comparing the number of nematodes that reach a spherical test region at the chemoattractant concentration peak with the number of those that reach a symmetrically placed control region in a low-concentration domain.

The chemotaxis efficiency is quantified using the chemotaxis index

$$CI(t) = \frac{n_t(t) - n_c(t)}{n_t(t) + n_c(t)}, \qquad \textbf{[S7]}$$

where $n_t(t)$ and $n_c(t)$ denote the number of nematodes that reached the test and control regions, respectively, during the time interval $[0, t]$. The simulation of a nematode trajectory is terminated when the nematode enters either the test or the control region [in 2D laboratory experiments these regions usually contain anesthetic to immobilize the nematodes (8)].

The spatial concentration of chemoattractant is given by a 3D Gaussian distribution

$$C \sim \exp\left(-r^2/2\sigma^2\right) \qquad \textbf{[S8]}$$

with the peak position at a distance $W = 36L$ from the starting point and the width $\sigma = 0.4W$. The diameter of the test and control regions is $D = 10L$. For the worm length $L = 1$ mm, the starting point is thus at a distance 3.6 cm from the chemoattractant concentration maximum, and the test and control regions have a 1-cm diameter (similar to the geometry of 2D experiments in a Petri dish). A sample trajectory of a swimming nematode reaching the test region is shown in Fig. S2*B*.

Fig. S3 depicts the chemotaxis index Eq. **S7** for two cases: (*i*) burrowing nematodes (no transverse slip) and (*ii*) swimming *C*-shaped nematodes. The results show that the chemotaxis index is

significantly greater than zero for both burrowing and swimming, indicating a clear trajectory bias toward the chemoattractant concentration peak. Moreover, the chemotaxis efficiency of burrowing and swimming nematodes is approximately the same; the burrowing nematodes, however, are able to reach the chemoattractant more quickly (and thus saturate the chemotaxis index *CI* at shorter times) than their swimming counterparts, due to a higher speed of motion.

The similarity of the saturation values of *CI* in burrowing and swimming results from two compensating effects: (*i*) The chemical signal Eq. **S2** is weaker in the swimming case because, as a result of their lower velocity, swimming worms detect a smaller time variation in chemoattractant concentration and (*ii*) the directional persistence length λ_p is larger for swimming trajectories, because of lower turn effectiveness (Fig. 7). The smaller time variation $dC/dt = \nabla C \cdot \mathbf{v}$ (where $\mathbf{v}$ is the nematode velocity) produces a weaker chemotaxis-response signal, Eq. **S2**, whereas the larger persistence length λ_p results in an increased systematic trajectory drift (relative to the diffusive random-walk component) toward larger chemoattractant concentrations. The balance between these two effects results in a similar number of nematodes reaching the test region for both cases considered.

According to our additional simulations (not shown), *CI* for burrowing and swimming is comparable to the value for crawling nematodes in an analogous 2D geometry. However, we also find that in 3D geometry a much larger fraction of nematodes escape without reaching either the test or the control region.

Chemotaxis of *C. elegans* in 3D environments was experimentally demonstrated in refs. 9 and 10. However, to our knowledge, the formulation presented here is a unique quantitative analysis that takes into account a realistic description of nematode movements and swimming mechanics.

1. White JG, Southgate E, Thomson JN, Brenner S (1986) The structure of the nervous-system of the nematode *Caenorhabditis elegans*. *Philos Trans R Soc Lond B Biol Sci* 314:1–340.
2. Altun ZF, Hall DH (2009) Muscle system, somatic muscle. *WormAtlas*, 10.3908/wormatlas.1.7.
3. Ugural AC, Fenster SK (1997) *C. elegans II* (Cold Spring Harbor Lab Press, Cold Spring Harbor, NY), 2nd Ed.
4. Pierce-Shimomura JT, Morse TM, Lockery SR (1999) The fundamental role of pirouettes in *Caenorhabditis elegans* chemotaxis. *J Neurosci* 19:9557–9569.
5. Lockery SR (2011) The computational worm: Spatial orientation and its neuronal basis in *C. elegans*. *Curr Opin Neurobiol* 21:782–790.
6. Celani A, Vergassola M (2010) Bacterial strategies for chemotaxis response. *Proc Natl Acad Sci USA* 107:1391–1396.
7. Bargmann CI, Horvitz HR (1991) Chemosensory neurons with overlapping functions direct chemotaxis to multiple chemicals in *C. elegans*. *Neuron* 7:729–742.
8. Nishino A, Sato F, Ito K, Matsuura T (2015) Extension of the established period of diacetyl adaptation by oxygen intermediates in the nematode *Caenorhabditis elegans*. *Comp Biochem Physiol A Mol Integr Physiol* 184:156–162.
9. Beron C, et al. (2015) The burrowing behavior of the nematode *Caenorhabditis elegans*: A new assay for the study of neuromuscular disorders. *Genes Brain Behav* 14:357–368.
10. Pierce-Shimomura JT, et al. (2008) Genetic analysis of crawling and swimming locomotory patterns in *C. elegans*. *Proc Natl Acad Sci USA* 105:20982–20987.

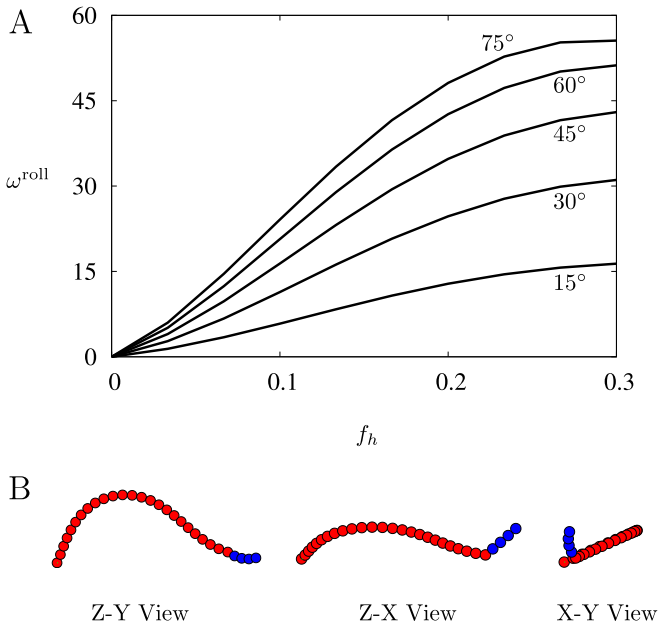

Fig. S1. (*A*) Roll rotation rate per undulation period ω^{roll} vs. head-length fraction $f_h = l_h/L$ for a *C*-shaped nematode performing curvature-modulated head tilt with maximal head tilt angles $\theta^{\max}$ as labeled. (*B*) *z–y*, *z–x*, and *x–y* views (from *Left*) of a swimming nematode tilting its head at a maximal angle of 45°. The blue circles mark the chain section that is tilted.

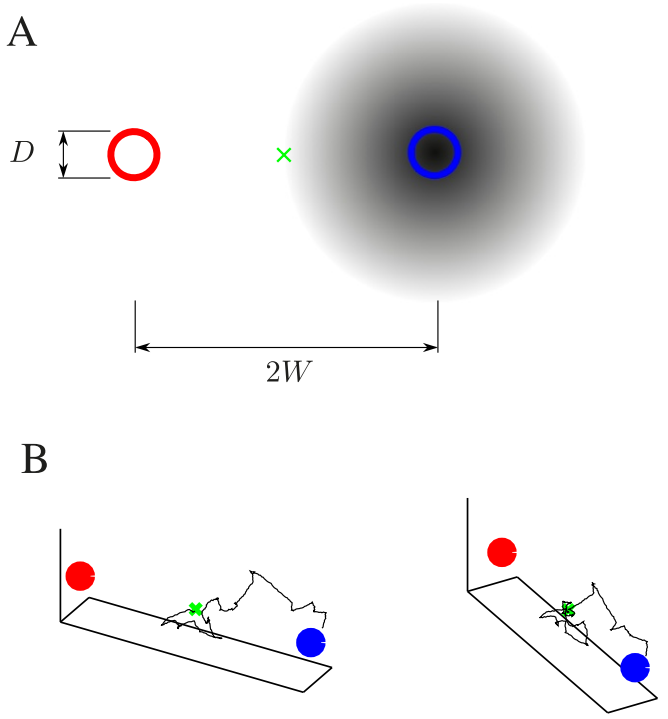

Fig. S2. (*A*) Top view of the simulated chemotaxis assay in 3D. Nematodes are initialized with a random orientation at the green symbol × located midway between the position of a Gaussian chemoattractant concentration peak (*Right*) and a spherical control region represented by the red circle (*Left*). The blue circle (*Right*) represents a spherical test region. (*B*) Views of a simulated path followed by a chemotaxing *C. elegans* in a 3D fluid.

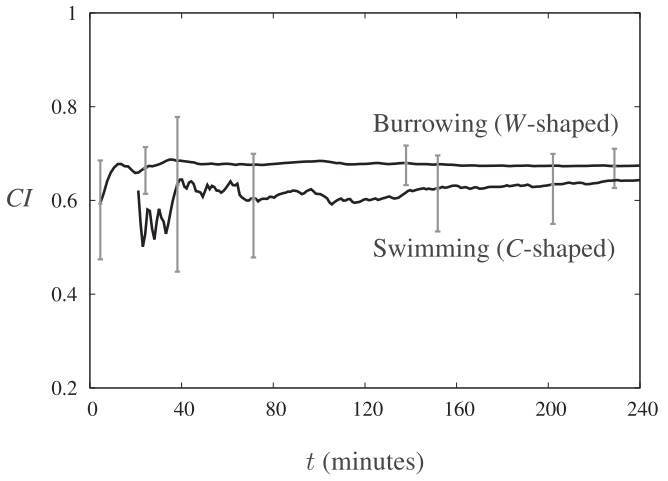

Fig. S3. Chemotaxis index *CI* vs. time for burrowing and swimming nematodes in 3D. The sensing parameters for the burrowing and swimming cases are the same, but the undulation frequency of the swimmer is four times larger than the undulation frequency of the burrower.

Table S1. System parameters for 3D simulations of chemotaxis of burrowing and swimming *C. elegans*

Parameter	Name	Value
α_s'	Chemoattractant sensitivity parameter	5 s/ mm
r_s^0	Turn initiation rate	10 turns/min
r_s^H	Upper turn-rate saturation limit	15 turns/min
r_s^L	Lower turn-rate saturation limit	5 turns/min
r_τ^0	Roll initiation rate	37 rolls/min
ϵ	Memory time constant	$1.6\,s^{-1}$
A_1/q	Forward mode normalized amplitude	1
f_b	Burrowing gait frequency	$0.44\,s^{-1}$
f_s	Swimming gait frequency	$1.75\,s^{-1}$
$q_{\text{burro}}L$	Burrowing gait normalized wavevector	9
$q_{\text{swim}}L$	Swimming gait normalized wavevector	5.5
L	Worm length	1 mm

The chemoattractant sensitivity parameter $\alpha_s' = \alpha_s/\nabla C|_{r=\sigma}$ is normalized by the maximal chemical concentration gradient located at $r = \sigma$. The memory time constant ϵ is chosen to correspond to $\sim$5 s half-decay response time of sensory neurons to the step increase of chemoattractant concentration (1).

1. Suzuki H, et al. (2008) Functional asymmetry in *Caenorhabditis elegans* taste neurons and its computational role in chemotaxis. *Nature* 454:114–118.

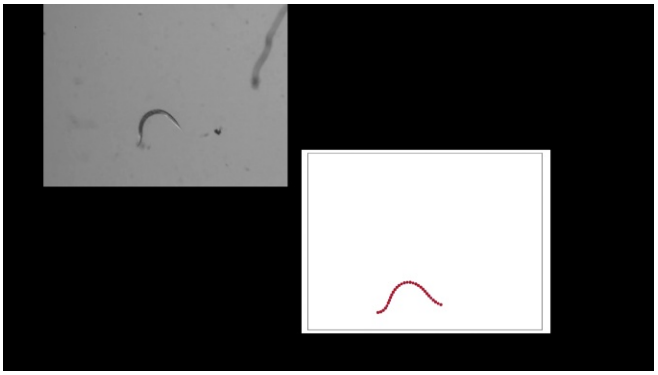

Movie S1. Planar turns of a swimming nematode. Shown is a comparison between a swimming wild-type *C. elegans* performing a series of planar turns and a matching simulation.

Movie S1

Movie S2. A roll maneuver of a swimming wild-type *C. elegans*. Within one period of undulation the nematode rotates by $\sim$90°.

Movie S2

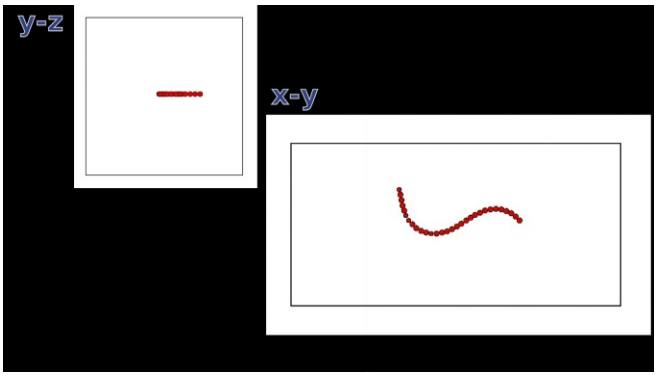

Movie S3. Simulation of torsional rolls of a swimming nematode. Shown are front and top views of a simulated swimming *C*-shaped nematode executing two consecutive three-mode rolls with the normalized torsion $\tau_0 L = 2$ and mode length $q\Delta s^{\tau} = 2.7$.

Movie S3

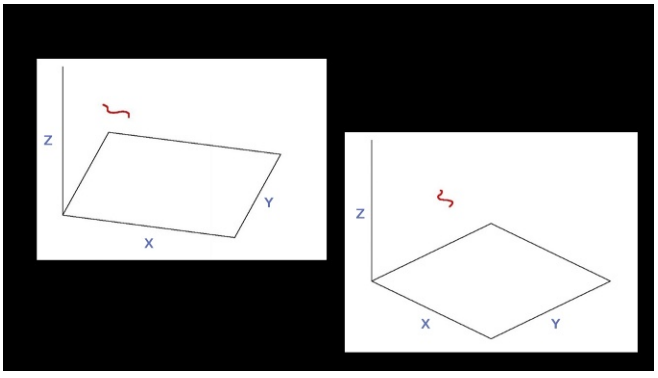

Movie S4. Simulation of 3D locomotion of a burrowing nematode. The nematode performs a sequence of planar turns and roll maneuvers; a combination of these maneuvers enables the nematode to explore 3D space.

Movie S4

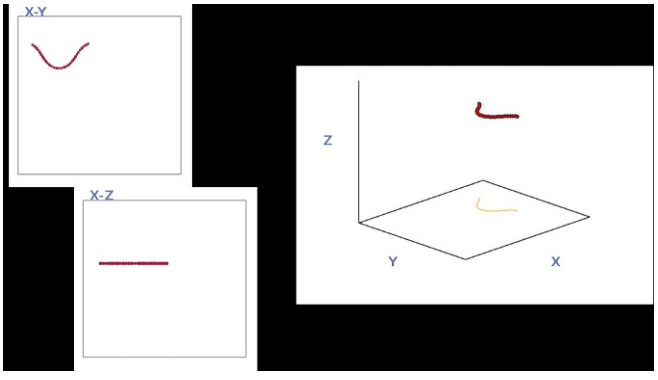

Movie S5. Simulation of 3D locomotion of a swimming nematode. Shown are isometric and stereoscopic views of a swimming nematode performing a sequence of planar turns and roll maneuvers.

Movie S5

Movie S6. Behavior of an adult *C. elegans* swimming near the bottom surface of a water pool. The nematode uses frequent roll maneuvers to reorient its undulation plane. The vertical orientation allows the nematode to remain suspended in the fluid, while the horizontal orientation enables turns in the plane parallel to the floor.

Movie S6